Relevance of Ground-based Electron Induced Electrostatic Discharge Measurements to Space Plasma Environments

Jennifer A. Roth,[1] Ryan Hoffmann,[2] J.R. Dennison,[3] and Jonathan R. Tippetts[4]

Utah State University Physics Department, Logan, Utah, 84322

Electron-induced electrostatic discharge (ESD) can lead to severe spacecraft anomalies. It is crucial to the success of space missions that the likelihood of ESD occurrence is understood and mitigated. To aid in predicting ESD occurrence, two models for electric field inside a dielectric material as a function of incident electron flux and energy were developed. An instrumentation system was designed to induce and detect ESD events. Because ESD events with a wide range of maximum current values can occur over a range of time intervals, multiple simultaneous detection methods were employed as charge was accumulated on a sample surface; these included monitoring of sample current and optical emissions from the sample surface. Data from ESD experimentation for James Webb Space Telescope was used to verify that the instrumentation system was effective in inducing and observing ESD. Two types of discharge events were observed during JWST testing: a sudden-onset, exponentially decaying current accompanied by luminescence in the optical data, and an arc or flash in optical data. JWST test results were applied to the electric field models developed to determine the threshold electric field for luminescence onset. The models were also applied to the JWST materials in five different space plasma environments to determine the accumulated electric field as a function of time, and to thereby predict the likelihood of sample luminescence in each location.

Nomenclature

b	=	range proportionality constant
D	=	dielectric material thickness
$\check{D}$	=	Dose rate
E_b	=	electron beam energy
F_{up}	=	electric field above charge layer
F_{down}	=	electric field below charge layer
J_b	=	electron beam current density
J_{out}	=	current density leaving material, measured current density
k_{RIC}	=	radiation induced conductivity proportionality constant
n	=	range exponent
q_e	=	charge of electron
R	=	charge layer depth, range
t	=	exposure time
$t_{ESD}^{up}, t_{ESD}^{down}$	=	exposure time at F_{ESD} above and below charge layer
Y	=	secondary electron yield
Δ	=	radiation induced conductivity exponent
ε_r	=	relative dielectric constant
ρ_m	=	mass density
Σ	=	charge density (C/m^2)
$\sigma_{RIC}^{up}, \sigma_{RIC}^{up}$	=	radiation induced conductivity above and below charge layer

I.   Introduction

SPACECRAFT charging is responsible for over half of all spacecraft anomalies caused by space environment interaction.[1] Of the many plasma environment particles that interact with spacecraft surfaces, electrons are the largest contributor to overall spacecraft charging, due to their high mobility.[2] Without sufficient methods for charge

---

[1] Undergraduate Researcher, Physics Department, 4415 Old Main Hill Logan UT 84322, Student Member.

[2] Graduate Researcher, Physics Department, 4415 Old Main Hill Logan UT 84322.

[3] Professor, Physics Department, 4415 Old Main Hill Logan UT 84322, Member.

[4] Undergraduate Researcher, Physics Department, 4415 Old Main Hill Logan UT 84322.

dissipation, these electron interactions can lead to electrostatic discharge (ESD), which can cause anomalies ranging from phantom signaling across circuits to material degradation and even complete satellite failure. Therefore, understanding electron-induced ESD in spacecraft materials is crucial to constructing an electrically-stable spacecraft.

In order to gain this understanding, results of ground-based ESD testing must be appropriately extrapolated to predict ESD occurrence in space. For this purpose, we developed instrumentation to induce and observe ESD, and created a model for the electric fields within a material during such testing. If able to understand the charge accumulated, or equivalently the electric field induced, the likelihood of ESD occurrence could be predicted from experiments using the aforementioned instrumentation. The validity of modeling ESD in the space plasma environment using these ground-based techniques is investigated.

II.   Theory

In order to begin modeling the electric field inside a material due to electron beam bombardment, the amount of charge accumulated and dissipated over a given time interval must be established. Charge accumulation depends upon the nature of incident electrons and the electrical conductivity of the material. The energy distribution and flux density of incident electrons, as well as the time the material is exposed to the electrons, determine the magnitude of the charge and energy incident on the material. The conductivity of a material determines how the material responds to this influx of charge. Total conductivity is the sum of dark current (DC) conductivity, a temperature dependent material property, and RIC, an enhanced conductivity for materials submitted to radiation.

A.   Electrostatic Discharge (ESD)

Charge carriers in conductors, which have high DC conductivity, are highly mobile in the presence of an applied electric field. According to the semiclassical model of electron dynamics, this results from the partially filled valence and conduction bands in these materials.[3] When fully grounded, electrons deposited in conductors by the incident beam are rapidly transported to the large ground charge reservoir and the material remains electrically uncharged. However, conductor cannot be fully grounded in space, so the entire conductor surface where charge resides develops a voltage relative to the ambient plasma environment in a process known as absolute charging.[4] If absolute charging leads to a sufficiently large electric surface potential relative to the ambient plasma, discharges to space can occur.[5]

By contrast, good insulators have low conductivity due to electron bands which are completely full or completely empty.[3] Because insulators are not able to conduct charge rapidly, an insulator will not likely have a constant voltage across its surface. Instead, regions of high and low voltage can develop—a process known as differential charging.[4] Often differential charging occurs between regions that are shaded and regions in full sunlight.[4] Voltage differences across the surface of a dielectric, or voltage differences between metal and insulating surfaces can cause ESD. This type of arc discharge, across surfaces, is known as "flashover" discharge.[5] Flashover does not typically occur for homogeneous material surfaces under uniform irradiation.

Deep dielectric or bulk charging can also lead to ESD. Bulk charging occurs in dielectric materials or on insulated floating conductors as energetic electrons are deposited within a material.[4] If electrons are deposited at a faster rate than they are dissipated, an electric field, F, develops in the material as a result of net charge accumulation. If this electric field becomes larger than the electrostatic breakdown strength, F_{ESD}, arc discharging occurs through the material, an ESD event known as "punch-through" discharge.[4,5]

B.   Conduction Mechanisms

The transport of charge in an insulator is determined by the electronic band structure of the material and the spatial and energy distribution of the localized trap states at energies within the band gap. For intrinsic insulators without trap states, charge transport results from excitation of electrons from the valence band (VB) into the conduction band (CB), followed by net motion of the charge carriers in the direction of an applied electric field (see Figure 1a). For intrinsic semiconductors, where $k_B T$ is a significant fraction of E_{gap}, this excitation is predominantly thermal. For higher band gap insulators or lower temperatures, thermal excitation is supplanted by energy transfer from incident radiation such as high energy photon or charged particle fluxes. When these conduction electrons recombine with holes in the VB, most of the energy is released as a photon of energy $\leq E_{gap}$.

For extrinsic materials which have localized trap states near the CB edge, thermally assisted conduction occurs. Electrons excited into the CB travel in the direction of the applied electric field until they undergo inelastic collisions and decay into trap states, are subsequently thermally excited back into the CB, and
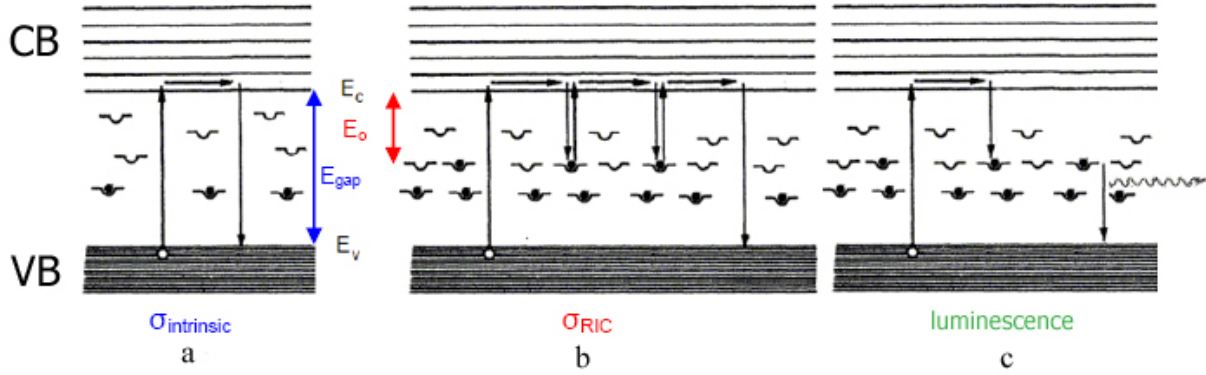
Figure 1. Conduction mechanisms in insulators. *(a) Conduction by direct excitation across the VB to CB. Thermally assisted hopping and variable range hopping. (b) Thermally assisted radiation induced conductivity. (c) Luminescence. Black dots and circles represent electrons and holes, respectively. Wavy line represents photon.*

eventually recombine with holes in the VB. Again, initial excitation into the CB is predominantly thermal for semiconductors. σ_{DC} for insulators typically follows an Arrhenius law of the form

$$\sigma(T) = \sigma_0 \, e^{-E_0/k_B T} \tag{1}$$

where E_o is an activation energy related to trap state energy depth below the CB edge that replaces the full band gap energy in a similar expression for thermally assisted extrinsic semiconductors.[3]

For typical insulators, traps near the CB edge are not populated and dark current conduction is dominated by thermally assisted hopping conductivity or variable range hopping mechanisms as electrons move from one trap state to adjacent trap state. As with intrinsic insulators, electrons can be excited into the CB by high energy incident radiation and then thermally pop in and out of trap states near the conduction band edge as they move in the CB under the influence of an applied electric field. This insulator conduction mechanism is referred to as radiation induced conductivity (RIC) and is shown in Figure 1b.[6] RIC is given by a simple power law

$$\sigma_{RIC}(T) = k_{RIC}(T) \, \dot{D}^{\Delta(T)}, \tag{2}$$

where both the proportionality constant, k_{RIC}, and the exponent, Δ, can be expressed as material dependant functions of T.[7]

The dose rate is defined as the total energy deposited in a material by the incident radiation per unit mass per unit time. The total energy deposited per unit area and unit time is the product, $J_b E_b$, divided by the charge per electron, q_e, and the unit mass equals the product of the mass density, ρ_m, and the range times unit area. Thus,

$$\dot{D} = \frac{J_b E_b}{\rho_m q_e R} = \frac{J_b}{\rho_m q_e b (E_b)^{n-1}} \tag{3}$$

where

$$R = b(E_b)^n \tag{4}$$

is a reasonable approximation to the energy dependence of the range[8] for incident energies from ~10^2 eV to 10^6 eV for tabulated data in the EStar database.[9] The parameters b and n are material dependant constants.

k_{RIC} is shown to be proportional to the rate of excitation from trap states into the conduction band, that is ~$e^{-E_o/k_B T}$. At lower temperatures, σ_{RIC} diminishes and electrons spend longer in the long-lived localized trap states. Longer residence time increases the probability that electrons in the trap states will recombine with holes in the VB and emit a photon of $\leq(E_{gap}-E_o)$. A distribution of trap states in energy will cause a distribution of emitted photon

3

energies. The process of radiation excitation to the CB, decay to a trap state, and subsequent decay to the VB with photon emission is referred to as luminescence. If excitation to the CB is caused by high energy electron radiation, it is referred to as electroluminescence.[10]

C. Electric Field Model

To first approximation, "punch-through" ESD will occur when internal electric fields, F, exceed the electrostatic field strength, F_{ESD}. We develop a simple model of the time-dependant electric field in terms of the incident electron beam energy, E_b, and current density, J_b, based on accumulated charge using a parallel plate capacitor approximation within a slab material (e.g., assuming sample thickness is much less than aerial dimensions). In the simple charge slab model used here, the dissipation or charge decay time, τ, is $\tau = \varepsilon_0 \varepsilon_r / \sigma$.
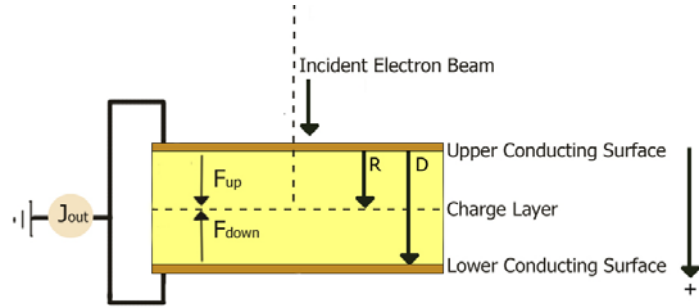

Figure 2. Simple model of electric fields within dielectric material.

Using the Bethe approximation for a non-penetrating electron beam, charge is deposited in a layer at a distance below the incident surface (or range), R, which depends on both the incident electron energy and the material. In the continuous slow down approximation (CSDA), the incident electron energy is dissipated at a constant rate, dE/dz, until all kinetic energy is lost at R.

For dielectric samples of thickness D and relative dielectric constant ε_r that are grounded on the top and bottom surfaces, electric fields develop above (F_{up}) and below (F_{down}) the deposited charge layer of charge density Σ, where

$$\begin{pmatrix} F_{up} \\ F_{down} \end{pmatrix} = \frac{\Sigma}{\varepsilon_0 \varepsilon_r} \begin{pmatrix} \left[1 - R/D\right] \\ -R/D \end{pmatrix}. \tag{5}$$

Such a model has been used for electron-irradiated polymer films.[11] If there is no charge dissipation, $\Sigma = J_b \cdot t$, the electric field increases linearly with time, and ESD occurs after an exposure time

$$\begin{pmatrix} t_{ESD}^{up} \\ t_{ESD}^{down} \end{pmatrix} = \frac{\varepsilon_0 \varepsilon_r \, F_{ESD} \, D}{J_b} \begin{pmatrix} \left[D - R\right]^{-1} \\ R^{-1} \end{pmatrix}. \tag{6}$$

For a more accurate representation of the induced electric fields, charge dissipation must also be considered, where the net charge density as a function of time is

$$\Sigma(t) = (J_{in} - J_{out})t = \left\{ J_b - \left[Y(E_b)J_b + J_{up} - J_{down} \right] \right\} t. \tag{7}$$

Here the first dissipation term in square brackets is for electron emission with a beam energy-dependant electron yield, Y, and J_{up} and J_{down} are the electron transport current densities to the upper and lower grounded surfaces, respectively, that can be written in terms of the internal electric fields as

$$J_{up} - J_{down} = \left(\sigma_{DC} + \sigma_{RIC}^{up} \right) F_{up} - \left(\sigma_{DC} + \sigma_{RIC}^{down} \right) F_{down} \tag{8}$$

using Ohm's law. We allow for both dark current conductivity, σ_{DC}, which is independent of incident dose rate, $\check{D}$, and radiation induced conductivity, σ_{RIC}, which by definition depends on $\check{D}$. Both σ_{DC} and σ_{RIC} are material and temperature dependant, as discussed in Section II.B.

Returning to Equations (1) and including charge dissipation via Equations (3) and (4), we find the coupled equations

$$\begin{pmatrix} F_{up} \\ F_{down} \end{pmatrix} = \frac{t}{\varepsilon_0 \varepsilon_r} \left\{ J_b \left(1-Y\right) - \left[\left(\sigma_{DC} + \sigma_{RIC}^{up}\right) F_{up} - \left(\sigma_{DC} + \sigma_{RIC}^{down}\right) F_{down} \right] \right\} \begin{pmatrix} 1 - R/D \\ -R/D \end{pmatrix}. \tag{9}$$

Solving Equation (7) for F_{up} and F_{down} and inserting Equations (5) through (8), we arrive at equations for F_{up} and F_{down} in terms of the incident beam energy, beam current density, and sample temperature:

$$\begin{pmatrix} F_{up}(E_b, J_b, T) \\ F_{down}(E_b, J_b, T) \end{pmatrix} = \frac{J_b t \left[1 - Y(E_b)\right]}{\left[D\left(\varepsilon_0 \varepsilon_r + \sigma_{DC}(T)t\right) + b\left(E_b\right)^n \sigma_{RIC}^{down}(T)t\right] + \left[D - b\left(E_b\right)^n\right] \sigma_{RIC}^{up}(E_b, J_b, T)t} \begin{pmatrix} \left[D - b\left(E_b\right)^n\right] \\ -b\left(E_b\right)^n \end{pmatrix}. \tag{10}$$

This provides an estimate of the electric field above and below the charge layer in a dielectric at some time, t.

III. Experimental Methods

Experimental techniques and apparatus were developed in order to: 1) approach the conditions of a space plasma environment, 2) develop electric fields in dielectric materials using incident electrons with known energy and current density, 3) and observe any ESD events induced by such electron bombardment.

A. Experimental Setup (Sample Preparation, Space Environment Simulation, and Inducing ESD)

In order to approach the infinitesimal particle density of space environments, experiments were performed in the USU Electron Emission Chamber, an ultra high vacuum (UHV) chamber maintaining a pressure of about 10^{-8} to 10^{-9} Torr. Samples were made to fit on 1-cm diameter cylindrical copper billets which were housed in a sample carousel. Samples of this size are small enough to fit within carousel, and large enough that for dielectric layers with thicknesses less than or equal to 100's of microns, the parallel-plate capacitor approximation is valid. The copper billet is connected to a grounded wire, and samples are attached to the billet using a conductive tape. This means that the bottom of each sample is always grounded. The top conducting layer of some samples is also grounded by attaching copper tape to the edge of the top surface and the side of the copper billet. Then, both the upper and lower conducting surfaces are grounded, as in the model developed above.

The USU Electron Emission Chamber is also equipped with liquid nitrogen feedthroughs and electrical heaters that allow the sample temperature to range from as low as 90 K up to 400 K. This is very useful in approaching on-orbit temperatures of spacecraft materials, which vary dramatically depending on the location and design of the craft.

Exposure to space plasma electrons of various energies and fluxes is simulated using an electron beam from a High Energy Electron Diffraction (HEED) gun. The HEED gun can be set to produce a stable beam with current densities ranging from about 0.1 nA/cm^2 to about 500 nA/cm^2, and energies from approximately 3 keV to 22 keV. The maximum spot size that can be achieved on a sample surface in the USU Electron Emission Chamber is about 9 mm in diameter. Before experimentation began, several measurements were taken to characterize the HEED beam. The HEED gun was conditioned to a specific energy, defocused, and then swept over a standard Faraday cup. Current measured from the Faraday cup was deconvoluded to determine the size and shape of the beam. This was done to characterize the beam, and to ensure that the spot size would cover the entire surface of each 1-cm diameter sample. Immediately before each test began, the HEED gun was conditioned to the appropriate beam energy and spot size. The beam was then directed at a Faraday cup and adjusted until the appropriate current density was obtained. Then the beam was directed at the sample for a given amount of time, and the sample was observed in order to detect ESD events.

B. ESD Detection Methods

ESD events are often difficult to detect because they occur over wide ranges of time intervals (from picoseconds to microseconds) and have maximum current values ranging from milliamps to tens of amps.[12] To detect as many events as possible during electron beam bombardment, several optical and electrical methods were used, as diagrammed in

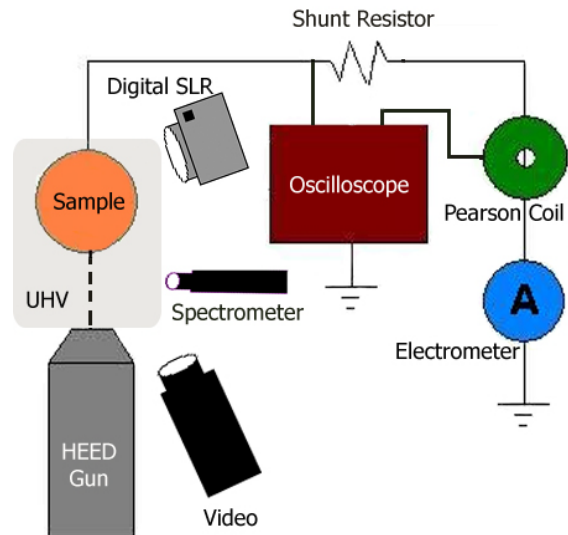
Figure 3. Diagram of ESD Detection Methods.

Figure 3. Three optical measurement devices recorded information about the sample surface during testing. The shutter of a Canon Digital Rebel XT SLR camera was opened for 30 second intervals to download an image of the sample. The camera reset for four seconds between each frame. Images were taken throughout the duration of each experiment. Optical data was also recorded with a Xybion low-level video camera. The camera was focused on the sample, and recorded grayscale video at a rate of 30 frames per second throughout the experiment. One end of a fiber optic cable was also positioned to collect light from the sample surface. The opposite end of the cable was connected to a spectrometer, capable of measuring light with wavelengths of 250 nm to 1100 nm at about 0.25 nm resolution. Spectra with 65-s integration times were taken throughout the duration of the experiment.

The sample current was monitored outside of the vacuum by a wire that is connected to a feed through. Three techniques were used to measure sample current. One of these instruments was a shunt ammeter. The shunt ammeter finds current by monitoring the voltage drop across a shunt resistor. The shunt ammeter can be set to use one of four metal-film resistors: 47 Ω, 100 Ω, 1000 Ω, 10,000 Ω. If the sample current detected by the shunt ammeter rises above a user-defined threshold, a Tektronix TDS 2040 Digital Storage Oscilloscope records a user-defined time interval of data about the trigger event. When the oscilloscope is triggered by the shunt ammeter, it also records data measured by a Pearson Electronics current monitor. This current monitor, also known as a "Pearson Coil," is simply a current transformer. A third technique for measuring current uses an electrometer/isolation amplifier board. The electrometer has a sampling rate of approximately 60 Hz. Unlike the current data for the oscilloscope, which is only recorded when triggered, the electrometer current data is recorded for the entire duration of each experiment. In order to determine if any gases were emitted from the sample as a result of ESD, a residual gas analyzer can be turned on during experimentation.

The final ESD detection method does not take place during experimentation. Optical microscope images of each sample surface are taken before and after ESD testing. A Canon Rebel XT Digital SLR camera is connected to a Zeiss microscope at 2.5x magnification. Photographs taken over the entire sample surface are stitched together in Photoshop. The images before and after testing are carefully reviewed and compared with one another. Particular attention is devoted to detecting scorch marks and other physical signs that suggest the occurrence of an ESD event.

Using each of these measurement devices, an ESD detection system was designed with optical sensitivities ranging from 250-1100 nm on time scales from 30 ms to 65 s, and with electrical sensitivity ranging down to about 0.1 nA for time scales as small as 2 ns. Such a versatile measurement system allows for more detailed observations of ESD events.

IV. Results for JWST Study

A series of ESD experiments were performed for James Webb Space Telescope materials. An overview of the results from these tests is provided in order to illustrate the effectiveness of the ESD instrumentation system and the validity of the electric field models.

The JWST is an infrared/near-infrared telescope scheduled to launch in 2013. It will reside near the second earth-sun Lagrange point (L2), where it will orbit the sun at the same rate as the earth. The craft will move in a halo orbit about L2, passing through several plasma regimes including the magnetosheath, magnetotail, and solar wind,[13,14] each with different electron fluxes and energies. It should also be noted that before the JWST reaches L2 it will pass through environments from LEO through GEO and past the moon.[14] It is crucial to the success of the JWST mission that the spacecraft be designed to withstand electron interactions in each of these regimes.

Tests were performed for four materials used as structural and optical/thermal materials for JWST. These materials include two bare and two gold-coated carbon fiber and fiberglass composites. The non-conductor coated samples have a 25-µm layer of epoxy on their top surface. The conductor-coated composites have a 25-µm layer of epoxy just below the top conducting surface. Tests were performed on these materials with beam energies of 22 keV and 7 keV, and with beam current densities of about 0.1 nA/cm^2 and about 1.0 nA/cm^2. Although the current density of 7-22 keV electrons in most JWST environments would likely be much lower than 0.1-1.0 nA/cm^2, the exposure time would be on the order of days, months, or years. In order to develop more practical ground-based techniques of simulating the space environment, the flux was increased, and the electron beam exposure time decreased to either 3600 s or 1000 s.

Under these conditions, two types of discharge events were observed during electron beam bombardment. One of these was a sudden-onset exponentially-decaying sample current accompanied by the release of intense blue photons. For the gold-covered samples, any glows seen occurred around the edge of the sample. For the composite materials, glows occurred in a football shape across about one-third of the sample surface. The initial magnitude of the glow current ranged from 1.7 times the electron beam current, to 121 times the electron beam current. Onset currents measured by the electrometer ranged from 0.14 nA to 23.82 nA. The still camera and electrometer showed

exponential decays with time constants on the order of about 10 minutes. Multiple glows did occur in some cases. In all five experiments where the glow extended to the end of testing, the glow ceased when the beam turned off. The coincidence of glows was very good between electrometer, video, and still camera data. Data from a glow during Test 50 is shown in Figure 4.
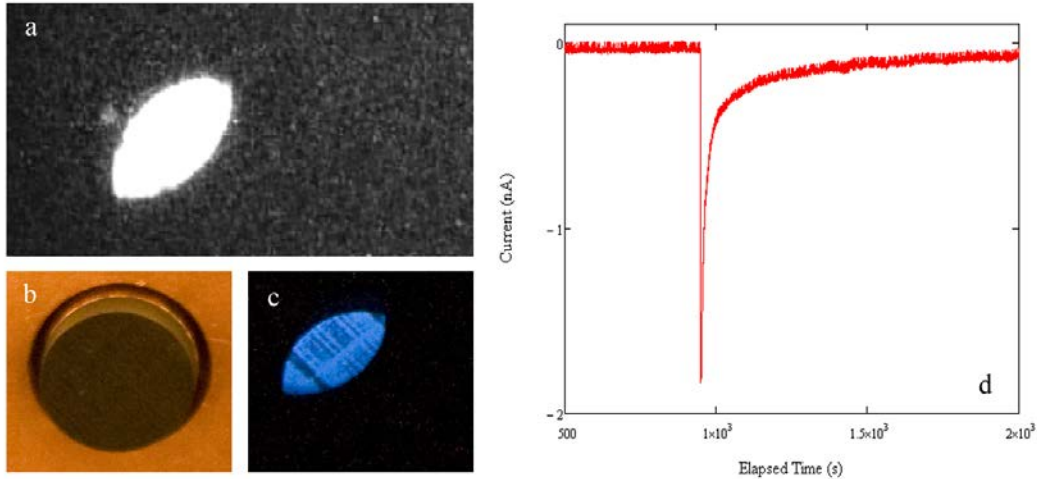

Figure 4. Glow discharge beginning at 948 s during Test 50. *a) Frame recorded by video camera at the time of the glow onset. Digital SLR images of the sample b) in full light before testing, c) at the time of the luminescence. d) Graph of sample current vs. time recorded by electrometer.*

The second type of discharge event was an arc discharge, characterized by a sudden spike in current and an intense flash of light. The oscilloscope traces show that these arcs occurred over time intervals of about 0.2 µs to 1.3 µs with peak currents ranging from about 5 mA to 150 mA. The energies of the arcs observed ranged from approximately 0.01 µJ to 1463 µJ. In four of the five tests where arcs occurred outside of a glow, these arc currents were negative. For all five tests with arcs occurring during a glow, these arc currents were positive. Sometimes the oscilloscope would not trigger for an arc detected by the other two methods. However, there was good overall coincidence of arcs between electrometer, oscilloscope, and video data. An arc during Test 60 as observed by each instrument is shown in Figure 5.
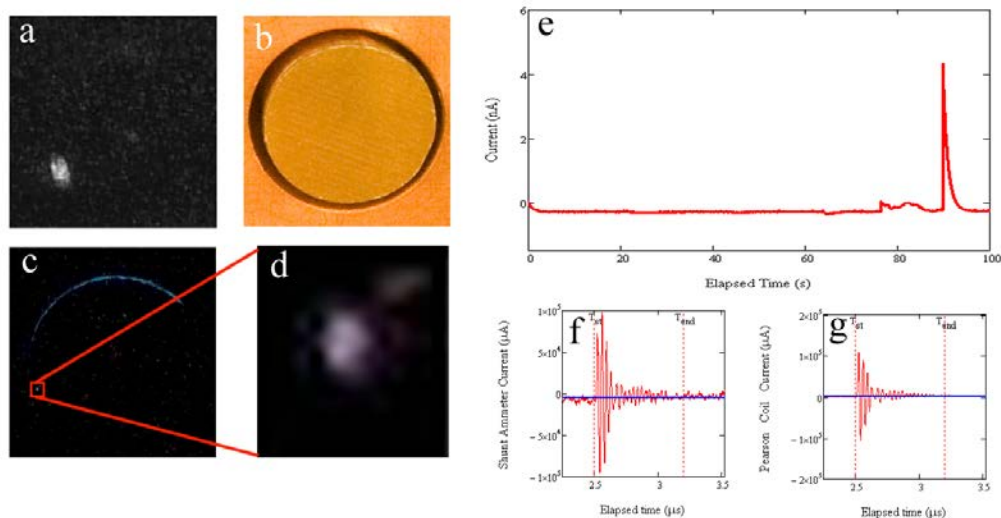

Figure 5. Arc discharge at 90 s during Test 60. *a) Frame recorded by video camera at the time of the arc. Digital SLR images of the sample b) in full light before testing, c) at the time of the arc, d) zoomed in on the area where the arc occurred. Graphs of current vs. time recorded by e) the electrometer f) shunt ammeter, g) Pearson Coil.*

7

V. Discussion

The results of the JWST testing demonstrated that the ESD instrumentation system is effective in observing ESD events of various intensities and obtaining electrical and spectral information for these events. Given the thickness of the epoxy layer and the energy of the electron beam, it appears that the layer of electrons was deposited in the epoxy in every test. The breakdown strength of the epoxy is approximately 20 MV/m.[12] If the electric field within the epoxy layer reaches this value, arcing is likely to occur. The data from the JWST experiments can be applied to the electric field models developed in Section II.C to determine the model's effectiveness in predicting ESD occurrence.

Using Equations (5) and (8) the electric fields above and below the charge layer were calculated at the time of the first arc occurrence, at the initial time of the glow onset, and at the end of the experiment. The values for the time of glow and arc occurrence are those observed using one of the current measuring devices (electrometer or oscilloscope). Blank cells indicate that no arc was observed with a current measuring device, although something may have been observed optically. Results using the model with no charge dissipation, Equation (5), appear in Table 1; calculations using the model that includes charge dissipation, Equation (8), appear in Table 2.

	Beam Parameters		Initial Glow Onset			First Arc Occurrence			Experiment Completion		
Test	E_b (keV)	J_b (nA/cm^2)	time (s)	F_{up} (MV/m)	F_{down} (MV/m)	time (s)	F_{up} (MV/m)	F_{down} (MV/m)	time (s)	F_{up} (MV/m)	F_{down} (MV/m)
50	22	0.058	948	6.8	-9.1	1429	10.3	-13.7	3600	25.9	-34.6
51	22	0.459	362	20.6	-27.5	406	23.1	-30.9	1000	56.9	-76.1
52	7	0.067	---	---	---	472	8.3	-0.9	3600	63.0	-6.9
53	7	0.702	---	---	---	---	---	---	1000	183.2	-20.2
60	22	0.485	1551	106.9	-111.1	76	5.2	-5.4	3600	248.1	-257.8
61	22	0.054	630	4.8	-5.0	379	2.9	-3.0	3600	27.6	-28.7
62	7	0.081	---	---	---	---	---	---	3600	80.4	-4.1
70	22	0.068	580	4.9	-6.5	621	5.2	-7.0	3600	30.4	-40.6
71	22	0.850	572	60.3	-80.6	432	45.5	-60.9	1000	105.4	-140.9
72	7	0.067	---	---	---	1399	24.5	-2.7	3600	63.0	-6.9
73	7	1.026	---	---	---	804	215.3	-23.7	1000	267.8	-29.5
80	22	0.499	880	62.4	-64.8	---	---	---	1000	70.9	-73.7
81	22	0.063	474	4.2	-4.4	---	---	---	3600	32.2	-33.5
82	7	0.168	---	---	---	---	---	---	3600	166.7	-8.5

Table 1. Electric field calculations above and below charge layer in epoxy, assuming charge dissipation.

	Beam Parameters		Initial Glow Onset			First Arc Occurrence			Experiment Completion		
Test	E_b (keV)	J_b (nA/cm^2)	time (s)	F_{up} (MV/m)	F_{down} (MV/m)	time (s)	F_{up} (MV/m)	F_{down} (MV/m)	time (s)	F_{up} (MV/m)	F_{down} (MV/m)
50	22	0.058	948	0.88	-2.22	1429	1.32	-3.30	3600	3.13	-7.86
51	22	0.459	362	2.54	-6.37	406	2.82	-7.09	1000	6.21	-15.59
52	7	0.067	---	---	---	472	1.48	-0.21	3600	7.42	-1.05
53	7	0.702	---	---	---	---	---	---	1000	12.36	-1.75
60	22	0.485	1551	10.36	-18.32	76	0.75	-1.33	3600	16.57	-29.30
61	22	0.054	630	0.70	-1.23	379	0.42	-0.75	3600	3.59	-6.35
62	7	0.081	---	---	---	---	---	---	3600	7.24	-0.46
70	22	0.068	580	0.64	-1.59	621	0.68	-1.70	3600	3.51	-8.81
71	22	0.850	572	6.12	-15.35	432	4.91	-12.31	1000	9.09	-22.79
72	7	0.067	---	---	---	1399	3.59	-0.51	3600	6.66	-0.94
73	7	1.026	---	---	---	804	10.97	-1.55	1000	11.56	-1.64
80	22	0.499	880	7.21	-12.76	---	---	---	1000	7.96	-14.08
81	22	0.063	474	0.61	-1.08	---	---	---	3600	4.15	-7.35
82	7	0.168	---	---	---	---	---	---	3600	10.14	-0.65

Table 2.   Electric field calculations above and below charge layer in epoxy, assuming charge dissipation.

For both models, the electric fields accumulated at the time of ESD events vary significantly from one test to another. At the time of glow onset, for instance, the magnitude of F_{up} ranged from as small as 4.2 MV/m up to 106.9 MV/m using the model without charge dissipation, and from 0.6 to 10.4 MV/m with the model that includes charge dissipation. The wide range of electric field values at times of breakdown could be due to differences in each of the samples tested. Due to the methods of manufacturing these materials, it is likely that the thickness of the epoxy layer is not consistently 25 µm for each sample, as was assumed in the models. Another technicality that was not considered in the model is the field enhancements that would occur from carbon fibers extending into the epoxy layer. There could be any number of fibers at a range of heights, which could have a significant effect on the value of the electric field within the epoxy layer.

There appears to be some correlation between the occurrence of glow events and the electric field below the charge layer at the end of experimentation. Luminescence or glowing occurred during every 22 keV experiment, and did not occur for any of the experiments with electron beam energy of 7 keV. Also, glows only occurred when $\left| F_{down} \right| > \left| F_{up} \right|$ and did not occur for experiments with $\left| F_{down} \right| < \left| F_{up} \right|$ at experiment completion. For the experiments using the higher beam energy and higher current density (51, 60, 71, and 80), glows occurred for electric field values of $6 < \left| F_{down} \right| < 18.5$ MV/m, which is not far from the breakdown strength of epoxy, 20 MV/m. It is likely that this breakdown strength is actually lower than 20MV/m for situations where the electric field is not increasing at a fast rate, meaning that the model values for electric field at luminescence onset are close to the expected breakdown field strength. For experiments using the higher beam energy and the lower current density (), glows occurred for electric field values of $1 < \left| F_{down} \right| < 2.5$ MV/m.

Using the values from Table 2, which assume charge dissipation, glows occurred for all tests in which the magnitude of F_{down} at experiment completion was greater than or equal to 6.4 MV/m. No glows were seen for experiments in which the magnitude of F_{down} was less than or equal to 1.8 MV/m. No experiments had final F_{down} magnitudes between 1.8 and 6.4 MV/m. This suggests that the magnitude of the electric field below the charge layer dictates whether or not glows can occur. There seems to be a threshold electric field between 1.8 and 6.4 MV/m, above which luminescence takes place.

Therefore, if the second model is applied to electron properties in a space plasma environment, the likelihood of glow occurrence can be predicted. To get a general idea of the accumulated charge in the epoxy in a space plasma environment, the electric fields in each material were estimated for the electron flux and energy values of five L2 or GEO space plasma environments: Geo-magnetic substorm, plasma mantle, plasma sheet, solar wind, and magnetosheath.

For conductor-coated materials, with approximately 0.11 µm of gold coating, electrons with energies ≤ 1 keV do not penetrate into the dielectric material. Electrons at these energies do not pose a threat for punch-through ESD occurrence, as no deep dielectric charging can occur. For materials without a top conducting surface layer, electrons with energies ≤ 1 keV are deposited at a shallow depth. Deep dielectric charging is diminished by surface charging effects such as electron backscattering and secondary electron yield. Therefore, for both the bare and conductor-coated materials studied, electrons with energies less than about 1 keV are unlikely to cause deep dielectric charging that would lead to punch-through ESD events.

For electron energies above a few keV, the electron yield decreases enough that surface effects are diminished and deep dielectric charging begins to occur. The range, or depth of the charge layer, increases with increasing energy. Electrons with energies greater than or equal to about 33 keV and above completely penetrate the 25-µm epoxy layer. Therefore, the electron energies of concern for dielectric charging within the epoxy layer are from about 3 keV up to about 33 keV. Electron flux values at energies of 7 and 22 keV were used to calculate electric fields after one hour and after one day in each of the five space plasma environments. The electric field values

American Institute
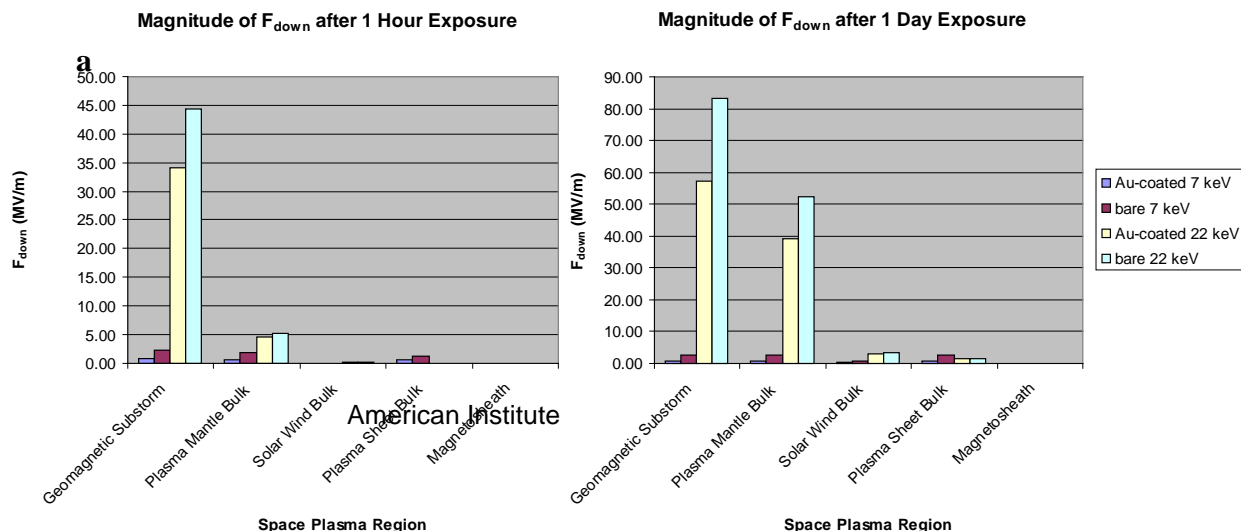
below the charge layer were found for both conductor-coated and bare epoxy samples and appear in Figure 6.

Figure 6. Estimated electric field below charge layer for bare and conductor-coated epoxy samples submitted to 7 keV and 22 keV electrons for a) 1 hour and b) 1 day.

As seen in Figure 7, electric field growth exhibits an asymptotic behavior after about one day in the geomagnetic substorm environment which results in virtually constant electric fields thereafter. This asymptotic behavior is seen after about a day in the plasma mantle bulk environment as well. For both conductor-coated and bare samples, the likelihood of glow occurrence is negligible for the magnetosheath environments; the electric field below the charge layer never rises above 0.02 MV/m, which is well below the glow threshold electric field (1.8 – 6.4 MV/m). There is a chance that luminescence will occur in the solar wind and plasma sheet environments. The largest F_{down} values reached in these regions are about 2.9 MV/m and 2.6 MV/m, which may or may not be above the luminescence threshold. There is strong evidence that geomagnetic substorm and plasma mantle environments cause both the bare and conductor-coated samples to glow, as both induce electric fields well above the threshold of 1.8-6.4 MV/m after just one hour. A larger conductive layer could reduce the energy of electrons entering the epoxy layer below, thereby reducing the electric field and hence the likelihood of luminescence.
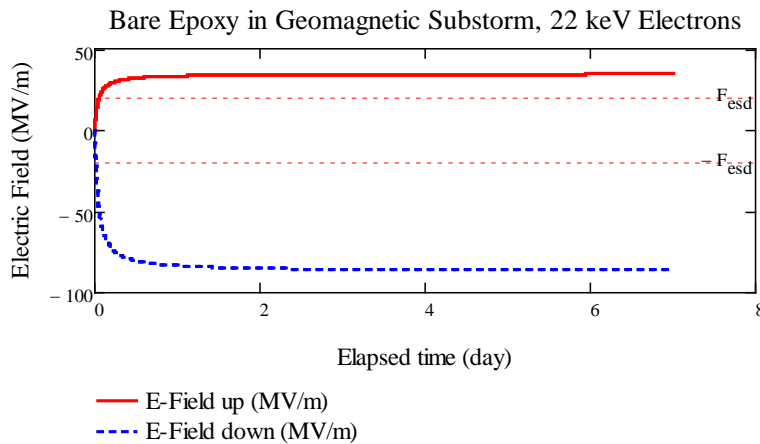

Figure 7. Electric field above and below charge layer for bare epoxy samples submitted to 22 keV electrons in a geomagnetic substorm environment.

VI.   Conclusions

Electron-induced electrostatic discharge events lead to anomalies that threaten the functionality and survival of spacecraft. In order to predict the likelihood of ESD occurrence in space, two models for electric fields within a dielectric material were developed. These included a simple model assuming no charge dissipation, and a more detailed model including charge dissipation. A ground-based instrument system was also developed to simulate the space plasma environment, to induce ESD, and to detect ESD events. Data from ESD experimentation for the James Webb Space Telescope verify that the instrumentation system was effective in inducing and observing ESD. Two types of discharge events were observed during JWST testing: a sudden-onset, exponentially decaying current accompanied by a glow in the optical data, and an arc or flash in optical data.

JWST test results were applied to the electric field models to investigate possible correlations between accumulated electric field and the occurrence of arc or luminescent phenomena. No apparent relation exists for arc occurrence and the electric fields calculated using the models developed. However, there does appear to be a luminescence threshold electric field between 1.8 and 6.4 MV/m as calculated by the model that assumes charge dissipation. Above this threshold field the sudden-onset exponentially decaying current that accompanies luminescence was observed, but was not seen below this threshold. The electric field model including charge dissipation was applied to the electron flux and energy values of five space environments to which the JWST will be

submitted (geo-magnetic substorm, plasma mantle, solar wind, plasma sheet, and magnetosheath.) In the plasma mantle, plasma sheet, solar wind, and geo-magnetic substorm environments there is a risk that luminescence could occur, since electric fields accumulate within and above the range of the luminescence threshold. These electric fields may be reduced by increasing the thickness of the conductive surface above the epoxy.

Future work includes refinement of the second model describing the electric fields above and below the charge layer in order to find some correlation between electric field and arc occurrence. A new model may also need to be developed for the non-conductor coated samples, which are not grounded on the top and bottom surfaces. Developing more accurate models through conduction theory and experimental verification will allow for more accurate estimations of ESD occurrence for spacecraft materials in orbit.

Acknowledgments

References

[1]H.C. Koons, et al., "The impact of the space environment on space systems," *6th International Spacecraft Charging Technology Conference*, Sep. 2000.

[2] R. Hoffmann, et al., "Low-Fluence Electron Yields of Highly Insulating Materials," *IEEE Trans. on Plasma Science*, Vol. 36, No. 5, 2008.

[3] N. W. Ashcroft and N. D. Mermin, *Solid State Physics*, 1st ed., Thomas Learning, USA, 1976.

[4] R.D. Leach and M.B. Alexander, "Failures and Anomalies Attributed to Spacecraft Charging," *NASA Ref. Pub. 1375*, 1995.

[5] B.F. James, O.W. Norton, and M.B. Alexander, "The Natural Space Environment: Effects on Spacecraft," *NASA Ref. Pub. 1350*, 1994.

[6]J. F. Fowler, "Radiation-induced Conductivity in the Solid State, and some applications," *Physics in Medicine and Biology*, Vol. 3, No. 4, 1959.

[7]J.R. Dennison, "Temperature Dependence of Radiation Induced Conductivity in Insulators," *AIP 20 CAARI*, 2009.

[8]NASCAP, NASA/Air Force Spacecraft Charging Analysis Program, v. 2.0, Science Applications International Corporation, available at URL: http://see.msfc.nasa.gov/ModelDB/ModelDB.htm.

[9]ESTAR, Stopping Power and Range Tables for Electrons [NIST database], URL: http://units.nist.gov/PhysRefData/Star/Text/ESTAR.html.

[10]V. Griseri, "Photoluminescence, recombination induced luminescence and electroluminescence in epoxy resin," J. Phys. D: Appl. Phys., Vol. 34, 2001.

[11]B. Gross, G. M. Sessler, and J. E. West, "Charge dynamics for electron-irradiated polymer-foil electrets," *Journ. App. Phys.*, Vol. 45, No. 7, July 1974.

[12] S.H. Voldman, *ESD: Physics and Devices*, 1st ed., Wiley, Hoboken, Chap. 1.

[13] J.I. Minow, et al., "Plasma Environment and Models for L2," *45 AIAA Aero. Sci.Mtg.*, Reno NV, 2004.

[14]S.W. Evans, et. al., "Natural Environment Near the Sun/Earth-Moon L2 Libration Point," *MSFC Report*, 2002, URL: http://www.aoe.vt.edu/~cdhall/courses/aoe4065/OtherPubs/SPECS/L2environment.pdf.